Fachtagung "Experimentelle Strömungsmechanik"
5.–7. September 2023, München

Experimental Investigation of the Wall-near Secondary Flow Field in a Low-Pressure Turbine Passage under the Influence of Periodically Incoming Wakes

Experimentelle Untersuchungen der wand-nahen Sekundärströmung in einer Niederdruckturbinen-Passage bei periodisch gestörter Zuströmung

Martin Bitter*, Tobias Schubert, Dragan Kožulović
University of the Bundeswehr Munich, Institute of Jet Propulsion,
Werner-Heisenberg-Weg 39, 85577 Neubiberg
*corresponding author: martin.bitter@unibw.de

Keywords*:* Rotor / Stator Interaction, Negative Jet, Passage Flow Field, Phase-Locked PIV

Abstract

Phase-locked Particle Image Velocimetry investigations were performed to investigate the flow field inside a low-pressure turbine cascade operating at engine-relevant high-speed and low-*Re* conditions. An application of phase-locked measurements was motivated by the disturbance of the flow field by periodically by incoming wakes. The effect of these wakes on the flow field itself and, in particular, on the exit flow angle was of interest for the work presented here. These wakes, which simulate the interaction of an upstream rotor row with the steady cascade in the wind tunnel, were produced by moving cylindrical bars passing upstream the steady cascade with a frequency of 500 Hz. The results quantify the production of turbulence intensity down-stream of the bars and its convection through a blade-to-blade plane at mid-span and in the regime of secondary flow close to an endwall. On time average, less underturning of the cascade was measured under unsteady conditions compared to steady inflow, especially in the secondary flow regime. An unavoidable blade passage phenomenon - the negative-jet effect – was extracted from the measurements. Finally, the results correlate well with comprehensive post-test numerical simulations.

Introduction

The establishment of high-lift blade designs in modern jet engines and the ongoing trend to reduce weight by lowering solidity in low-pressure turbine (LPT) vanes has triggered a lot of research on endwall flow in recent years. The main motivation is the significant contribution to overall losses due to high pressure gradients in the blade passage and thus intensified endwall flow. In the case of low aspect ratio LPT blades in which a larger range of the blade span is affected, the endwall losses are approximated to account for one third of overall losses, see Cui & Tucker 2016. Based on a numerical parametric design study in LPT cascades, Coull 2017 found that endwall losses can be decomposed into two major components: dissipation in the endwall boundary layer and induced losses by secondary flows, which scale with streamwise vorticity. According to Denton & Pullan 2012, the secondary flow itself exhibits several sources of loss, such as flow interactions inside the blade passage and downstream mixing losses. Particularly, the interaction of the passage vortex and the blade suction surface, resulting in the counter rotating vortex, was found to have a strong contribution to overall losses by

GALA e.V., Karlsruhe, Germany, ISBN 978-3-9816764-9-5

Cui & Tucker 2016 as well as Bear et al. 2018. The endwall flow development is also largely dependent on inflow conditions. The effects of periodically incoming wakes were investigated in the T106A and T106Div turbine cascades using measurements and (U)RANS simulation by Ciorciari et al. (2014, 2018). Both approaches have shown an attenuation of the secondary flow. In contrast to relatively small effects of incoming wakes, Volino 2014 found the influence of the inlet boundary layer to be much larger. Schubert & Niehuis 2021 came to a similar conclusion when evaluating the turbine cascade exit flow, however, they found the endwall flow development inside the blade passage is significantly affected by both factors, but in different manners.

Despite the vast research activity in recent years, the accurate prediction and reduction of endwall loss is expected to remain a challenge for many years to come, compare Denton & Pullan 2012. Aimed at providing a further step in the continued understanding of endwall flow and its determining factors, an extensive research program funded by the Deutsche Forschungsgemeinschaft (DFG) was launched in 2018 by four German university institutes, Engelmann et al. 2021. Within this conglomerate the Institute of Jet Propulsion of the University of the Bundeswehr Munich covered low-pressure turbine aspects at high-speed flow conditions. This paper is based on the design work and first experimental results of Schubert et al. 2021. They used a particular turbine cascade design to investigate the effects of boundary layer condition and periodically incoming wakes on the secondary flows and losses by means of extensive measurements and numerical simulation, see Schubert & Niehuis 2021 for CFD. The previous up- and downstream measurement results are extended by optical measurements inside the blade passage, which pose a far greater challenge in terms of experimental setup. The discussion of these results shall be the main part of this paper.

Setup & Methodology

Testcase: T106A Low-Pressure Turbine Cascade

The presented experiments were conducted using a linear cascade of the T106A low-pressure turbine profile. The key geometric- and flow parameters are summarized in Table 1. The turbine cascade is a redesign, which was specifically developed for endwall flow measurements under periodic inflow and high-speed conditions (M_{2th} = 0.59; Re_{2th} = $2 \cdot 10^5$). The blade profile geometry remains unchanged, though. The main improvements of the current cascade are a sufficiently thick endwall boundary layer and the ability to perform variations of the boundary layer conditions on this endwall. The challenge regarding the endwall boundary layer stems from a gap between the wind tunnel and the cascade endwalls, upstream of the blade passages. This gap, which is needed for the moving bar wake generator, enables a leakage flow driven by a negative pressure gradient. While the freestream flow is not affected, it can act as a boundary layer suction leading to weak secondary flow. To counteract this problem, the current cascade features an integrated split flat plate at part-span, which serves as a turbine endwall (marked in yellow in Figure 1). Using a modular composition of the aft

Geometric Parameters:	
Chord length ***C***	100 mm
Pitch-to-chord ratio ***P/C***	0.799
Aspect ratio ***H/C***	1.31
Flow Conditions:	
Mach number at exit M_{2th}	0.59
Reynolds number at exit Re_{2th}	$2 \cdot 10^5$
Design inflow pitch angle β_1	127.7°
Design outflow pitch angle β_2	26.8°
Turbulence intensity ***TI***	6.8%
Unsteady Inflow Conditions:	
Strouhal number ***Sr***	0.66
Flow coefficient Φ	3.8

Table 1: Geometric and aerodynamic conditions of the T106A linear turbine cascade.

GALA e.V., Karlsruhe, Germany, ISBN 978-3-9816764-9-5

plate, various measurement techniques can be implemented with manageable effort. The endwall boundary layer can be adjusted by misaligning the front plate with respect to the aft plate. During all measurements presented in this paper, the endwall boundary layer thickness was δ_{99} = 4.62 mm with a form factor of H_{12} = 1.86 at 45 % Chord *C* upstream of the blade's leading edge. A detailed description of the particular testcase design and an investigation of the effects of endwall boundary layer variations on the secondary flow and loss production can be found in Schubert & Niehuis 2021 and Schubert et al. 2021.

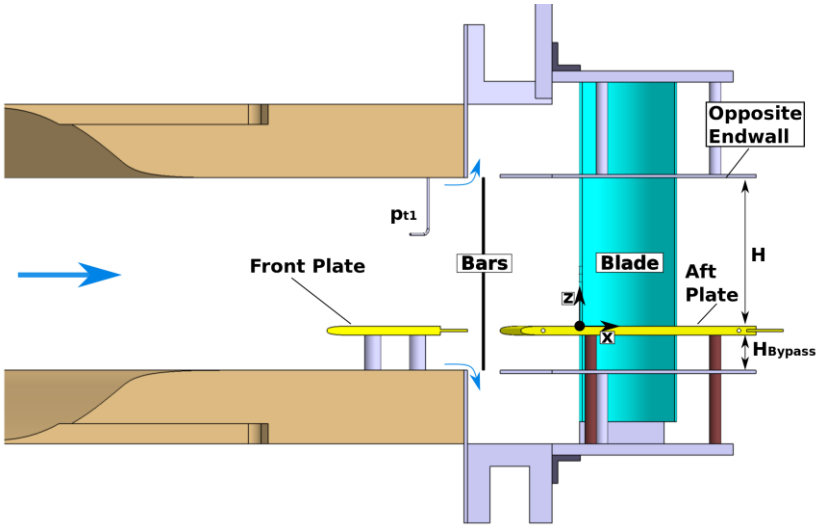

Figure 1: Illustration of the T106A test case featuring a split flat-plate-endwall (yellow) and moving bars upstream of the low-pressure turbine blades (cyan), adapted from Schubert et al. 2021.

Numerical simulations were utilized during the cascade design (pre-test CFD) as well as to support the experimental results (validated post-test CFD) with time-resolved flow data, especially in areas of limited accessibility. The simulations were performed using the URANS flow solver TRACE by DLR with the *k*-ω turbulence model by Wilcox 2004 and γ–$Re_{\theta t}$ transition model by Langtry & Menter 2005. The computational domain covers a single blade pitch with periodic boundary conditions. It is divided into an upstream block group encompassing the front plate, the moving domain containing two bar pitches, and a downstream block group which encompasses the blade passage and aft plate. The leakage flow is simulated by additional outlet panels at the bar gap boundaries. The blade passage is discretized using an *OCGH*-topology and low-Reynolds wall treatment (*y+1*), resulting in high boundary layer resolution. Sufficient spatial and temporal discretization is ensured by a sensitivity study, which leads to an overall number of nodes of approximately $8 \cdot 10^6$ and several time steps per moving domain period (two bar pitches) of 800. The flow conditions prescribed at the in- and outlet plane match the wind tunnel conditions in the experiment (M_{2th} & $Re_{2th} = f(T_{t1}; p_{t1}; p_3)$ and Tu_1). A detailed description of the computational approach can be found in Schubert & Niehuis 2021.

The key flow characteristics inside the T106A blade passage are illustrated by means of CFD in Figure 2. Here, axial slices of entropy generation rate and iso-surfaces of the Q-criterion

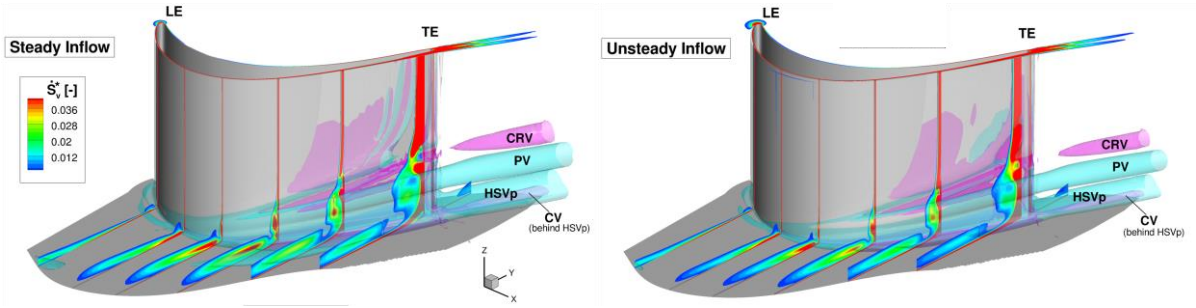

Figure 2. Simulated entropy generation rate per unit volume at several axial slices inside the T106A blade passage under steady (left) and unsteady inflow conditions (right), adapted from Schubert & Niehuis 2021. (HSVp – pressure-side branch of horseshoe vortex; PV – passage vortex; CRV – counter-rotating vortex; CV – corner vortex; LE – leading edge; TE – trailing edge).

GALA e.V., Karlsruhe, Germany, ISBN 978-3-9816764-9-5

(colored by streamwise vorticity indicating the sense of rotation) indicate loss production at midspan and the secondary flow region. In the 2D-flow region around mid-span the levels of loss production start off moderately in the predominately aft-loaded T106A. However, near the trailing edge ($x / C_x = 1$), strong adverse pressure gradients acting on the blade suction surface led to the formation of a separation bubble. Under unsteady inflow, wake-induced transition periodically forces the suppression of the separation bubble. This unsteady effect is visible in the time-averaged flow in Figure 2 by a lack of alternating vorticity on the rear suction surface. Near the endwall, strong transverse pressure gradients force the boundary layer fluid towards the suction surface. During this process, the flow is rolling up, is fed into the passage vortex, lifts off the endwall and finally impinges on the blade suction surface. In addition to the resulting high losses, the secondary flow can be well identified by overturning close to the endwall and corresponding underturning at the upper edge of vortex interaction. In case of unsteady inflow, the interaction of the wakes with the endwall boundary layer periodically delays the development of passage vortex. This leads to the attenuation of the secondary flow further downstream and hence a reduction of the secondary losses.

Experimental Investigations

The experiments were conducted at the High-Speed Cascade Wind Tunnel (HGK) of the University of the Bundeswehr Munich, see Niehuis & Bitter 2021. The facility allows aerothermodynamic investigations of turbomachinery components at engine-relevant Mach and Re numbers, which can be varied separately. For this reason, the main components of the HGK are enclosed by a large plenum chamber with 4 m in diameter and 12 m in length. The absolute pressure in this plenum chamber can be evacuated down to 4 kPa or pressurized up to 1.2 MPa. The wide pressure range together with the large test section dimensions make it possible to perform aero investigations on relatively large test specimens, even for low operating Reynolds numbers. This mitigates the relative influence of probe-based measurement techniques on the flow field, especially at high downstream Mach numbers typically encountered on a turbine cascade, see Börner et al. 2018.

The baseline cascade has a long research history in the lab and the aerodynamic performance is well known under various operating conditions – but without an additional side wall, see e.g., Kampisch et al. 2000, Blaim & Niehuis 2012 or, Kirik & Niehuis 2015. The cascade specifications are exactly as used for the numerical simulation outlined in the previous section and as given in Table 1.

The HGK's test section can be equipped with a linear wake generator which produces periodically incoming wakes of up to 500 Hz at the linear cascade's inlet, see Acton & Fottner 1996. The periodically incoming wakes are generated by steel bars with a diameter of 2 mm, i.e., 111% of the T106A trailing edge diameter. The moving bar plane, which runs parallel to the blade passage inlet plane, is located 86% C upstream of the blade leading edge. The ratio of bars to blade count is two-to-one, i.e., $P_b / P = 0.5$ and the bar speed is $v_b = 20$ m/s which leads to a bar passing period of 0.002 s. Previous experimental and numerical studies of the T106A turbine cascade have shown that increased bar velocity (higher Sr and lower Φ) results in intensified effects on the secondary flow, Ciorciari et al. 2014. However, within a reasonable range of unsteady inflow parameters, the observed trends remain unchanged.

The aim of measuring a highly resolved passage flow field with phase-locked Particle Image Velocimetry (PIV) in close vicinity to a parallel wall and under severe vibrations of the wake generator presents a big experimental challenge. These circumstances necessitated the optical access towards the flow passage via a rod endoscope through several side walls of the test specimen.

GALA e.V., Karlsruhe, Germany, ISBN 978-3-9816764-9-5

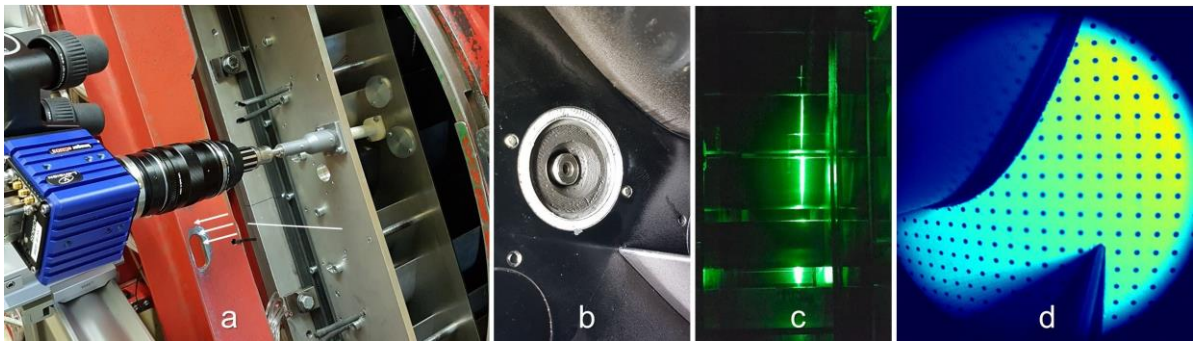

Figure 3: PIV setup for wall-near flow measurements inside the T106A linear cascade: a) endoscopic camera setup into the passage; b) optical access into the flow channel; c) PIV laser sheet at $z / H = 0.2$; d) camera calibration target in the field-of-view.

Figure 3 highlights some impressions from the experimental setup installed in the HGK test section. The sCMOS camera (5.5 Mpx, Fig. 3a) was connected to a 35 mm optical lens and a 220 mm long rod endoscope with 8 mm diameter and 67° opening angle. The optical access into the passage from the opposite endwall is shown in Figure 3b. The light sheet formed by an Innolas Spitlight 1000 Nd:YAG LASER was introduced into the setup from downstream the cascade, which unfortunately led to the formation of shadowed areas and impeded the measurement of the entire passage. A calibration plate (Fig. 3d) with 2 mm dots arranged with 10 mm constant spacing was specifically tailored to the blade passage to calibrate the PIV images and compensate for the strong image distortions relsulting from the short working distances in the 2 measured PIV sections at $z = 65.5$ mm ($z / H = 0.5$, “mid-span”) and $z = 26.2$ mm ($z / H = 0.2$, “wall-near”) .

Since the main intention of the PIV measurements was the investigation of the interaction of the passage flow field with the periodically incoming wakes, phase-locked PIV measurements according to Bitter & Niehuis 2019 were performed. A set of 10.000 PIV images was recorded at 11 Hz while the dominant bar passing frequency was 502 Hz. Since both frequencies were de-coupled, the flow field was measured with the bar being at random pitchwise positions upstream the reference blade. A correspondance between the geometric bar pitch P_b and the temporal bar period t_{BP} was determined according to Figure 4. The position, at which the bar was located horizontally upstream of the leading edge served as reference, both, in the numerical and the experimental investigations. A length of 17.3 mm (40 mm P_b - 22.7 mm as

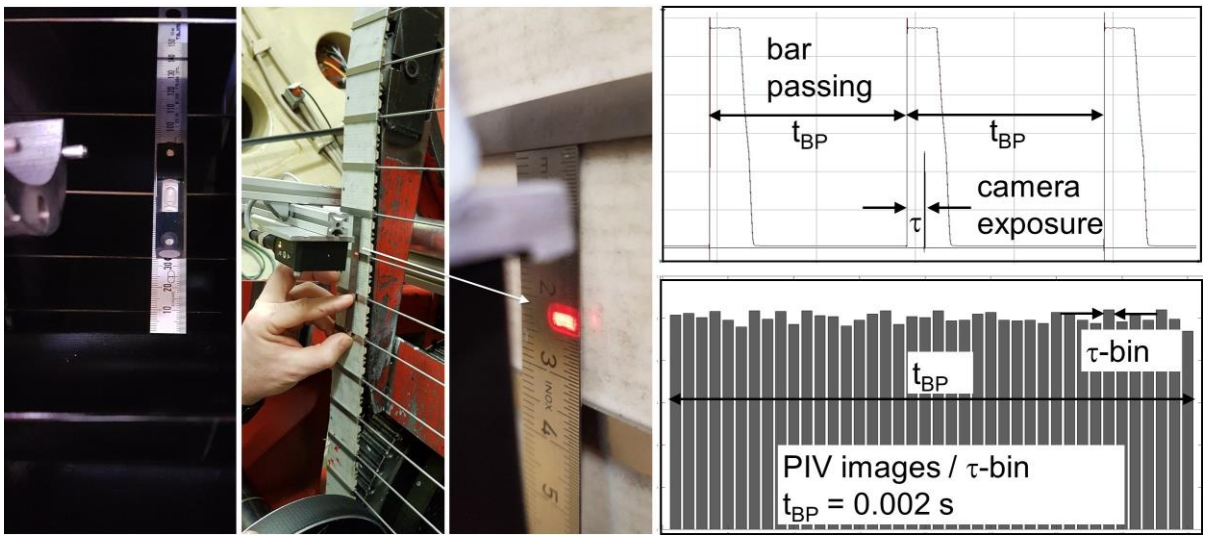

Figure 4: Alignment of the spatial bar position with the temporal trigger signals from the bar counter and the camera exposure; PIV images, captured over 1 bar period t_{BP} at random τ, were collected in τ - bins of arbitrary bin width (here: τ - bins = $5 \cdot 10^{-5}$ s) and finally phase averaged.

GALA e.V., Karlsruhe, Germany, ISBN 978-3-9816764-9-5

indicated by the red optical bar counter signal in Fig. 4) divided by P_b results in a relative offset of the reference position from the last bar passing event, i.e., $\tau / t_{BP} = 0.434$. Since the camera exposure signals were randomly distributed over 1 t_{BP}, the PIV images were re-sorted into τ-bins in an individual post-processing. The distribution in the lower right of Figure 4 shows the statistically even distribution of PIV images per τ- bin. This sorting can be adjusted on demand. The more bins chosen, the higher the temporal resolution of the bar wake passing through the passage, but the lower the number of PIV images per bin for averaging the flow field. For the following discussions, 20 bins were chosen.

Discussion of Results

Ensemble-averaged Passage Flow Field

At first, the ensemble-averaged passage flow fields at “mid-span” and “wall-near” are discussed inside one blade passage with and without the influence of the periodically incoming wakes in Figure 5 (mid-span) and Figure 6 (wall-near), respectively. The left-hand side of each figure represents the “steady” absolute velocity field ensemble-averaged over the entire image series without periodic perturbation. The center plot shows the corresponding periodically disturbed “unsteady” case. The value for normalization was the theoretic exit velocity at M_{2th} = 0.59, i.e., V_{2th} = 199.1 m/s. On the right, the absolute flow field difference between steady and unsteady conditions is highlighted color-coded (blue – positiv, red – negative). A circular appearing shape of the flow field results from the endoscope’s field of view. A wider field of view at z / H = 0.2 is the consequence of the 67° opening angle.

Both figures indicate that the absoute velocity in the passage is slightly lower under unsteady operation resulting in a slightly negative delta. In accorddance Bitter & Niehuis 2019, the presence of the moving bars introduces total pressure losses and a stronger turbulence level. In a real engine, these total pressure losses may be even higher if real rotor blade losses are encountered. This effect seems to be more pronouced in the wall-near plane but is also noticeable at mid-span. In the white areas, especially close to the suction side of the upper

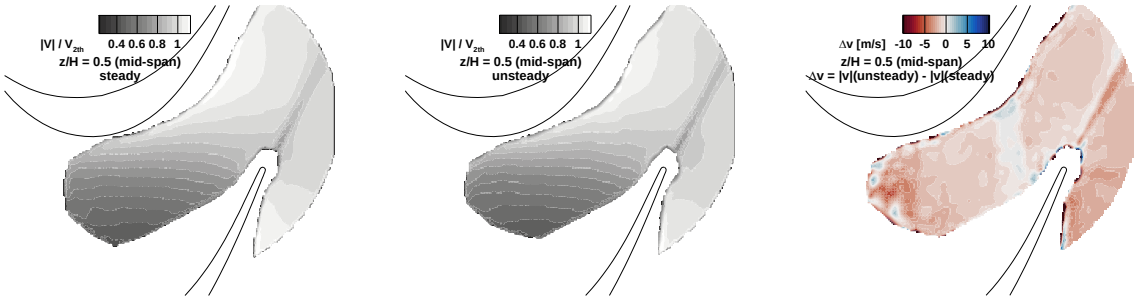

Figure 5: Ensemble-averaged passage flow field at z / H = 0.5 (mid-span) under steady (left) and unsteady (middle) inflow conditions; right: $\Delta|V|$ between steady & unsteady inflow conditions.

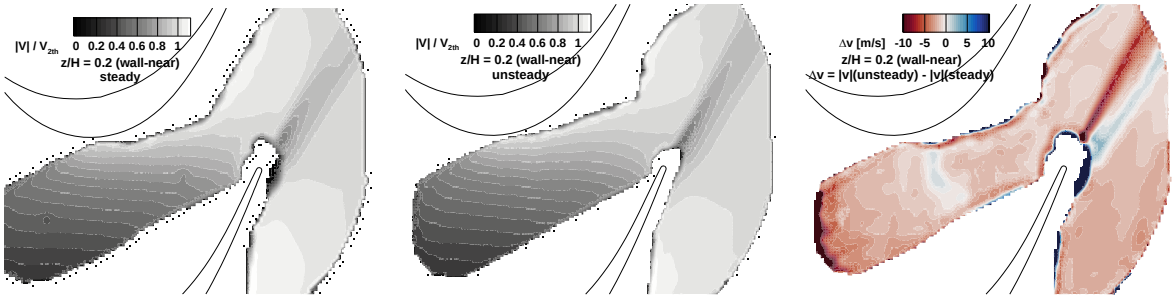

Figure 6: Ensemble-averaged passage flow field at z / H = 0.2 (wall-near) under steady (left) and unsteady (middle) inflow conditions; right: $\Delta|V|$ between steady & unsteady inflow conditions.

GALA e.V., Karlsruhe, Germany, ISBN 978-3-9816764-9-5

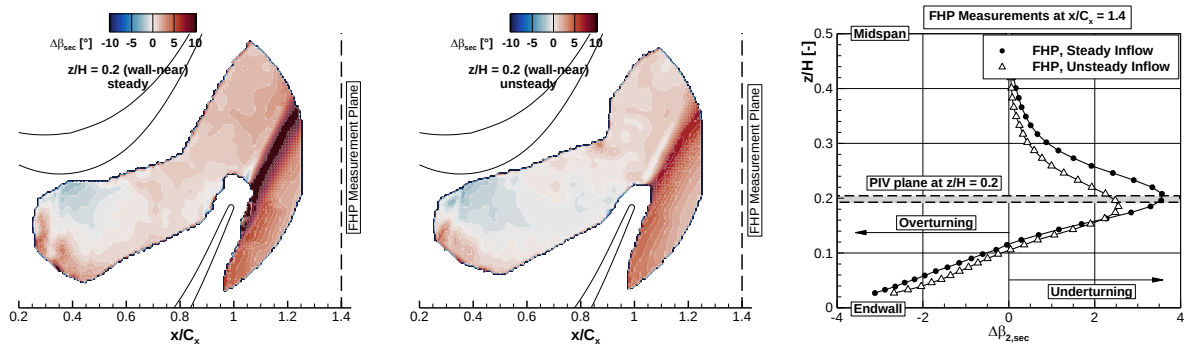

Figure 7: Ensemble-averaged velocity flow angle difference (with respect to mid-span) at z / H = 0.2 under steady (left) and unsteady (middle) inflow conditions; right: integral exit velocity angle difference (with respect to mid-span) measured with a five-hole probe at x / C_x = 1.4 downstream the cascade.

blade, the data availability is limited due to strong direct LASER reflections as a consequence of the illumination from the back. Unfortunately, the area which is crossed by the secondary vortex system coincides with this region, compare Figure 2.

The major time-averaged impact of the moving bar wakes is present at the wake flow downstream of the turbine blades as highlighted in Figure 7. The figures show the reduction of the cascade outflow angle in the wall-near plane with with respect to the outflow angle at mid-span. This delta is a consequence of the relative velocities in the complex secondary vortex system close to the endwall, compare Figure 2. A positive delta has the consequence that the flow turning of the turbine blade is reduced (named “underturning”). As to be seen, the flow angles increase by more than 10 degrees under steady inflow conditions but slightly less under unsteady inflow. This effect is confirmed by five-hole probe (FHP) measurements further downstream of the cascade. The FHP measurement plane at x / C_x = 1.4 is indicated by the dashed lines. The FHP measurements show an integral value of the $\Delta\beta$ integrated over one complete blade pitch and are plotted for various blade height positions z / H up to the mid-span area. Nevertheless, the probe measurements indicate the same trends as PIV does. The FHP results motivated the PIV measurements at z / H = 0.2 as the underturning effect is the strongest in this plane. The blade’s aerodynamic performance suffers from high underturning (and also overturning) since the successive blade rows experience severe off-design conditions with respect to their design inflow velocity triangles. Hence, the knowledge of the amount of over-/underturning must be considered in the design of a turbomachinery stage.

Periodic Wake Effect on the Wall-near Passage Flow Field

According to Bitter & Niehuis 2019, the cylindrical bars from the wake generator produce around 20 % turbulence intensity increase in their core wake at similar operating conditions compared to the present investigations. Further downstream, these levels are mixed out. As given in Table 1, the main flow turbulence intensity was about 6.8 % in the experiments performed here. Figure 8 shows the temporal behaviour of the wall-near passage flow field at four consecutive time steps τ of one bar passing period t_{BP}. The top row shows the normalized absolute velocity fluctuation $|V|' / V_{2th} = (\overline{|V|}(\tau) - \langle|V|\rangle / V_{2th}$, whereas $\overline{|V|}(\tau)$ is the mean absolute of a τ-bin and $\langle|V|\rangle$ is the ensemble averaged flow field over the entire time series normalized with V_{2th} = 199.1 m/s. The bottom row highlights the corresponding velocity field angle in the passage. Every 8th velocity angle is indicated by an arrowhead. The displayed data was averaged from about 470 PIV images per τ-bin. At $\tau / t_{BP} = 0$, one random bar is located horizontally upstream the reference blade’s leading edge. On average, the bar produces a wake deficit as indicated by blue color. According to the inflow velocity triangles, the bar wake reaches the leading edge of the blade slightly later in time. The correspondig phase lag between bar position and wake entry into the passage was calculated to be about -

GALA e.V., Karlsruhe, Germany, ISBN 978-3-9816764-9-5

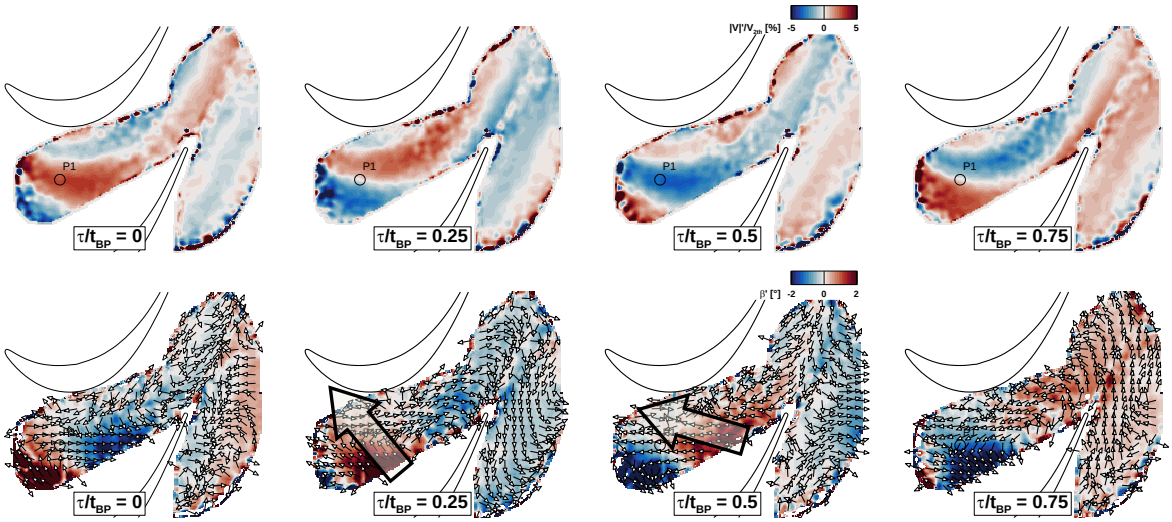

Figure 8: Effect of the bar wake on the secondary flow (z / H = 0.2) in the T106A turbine passage. Top row: Evolution of the bar wake velocity deficit for four normalized bar passing time steps. Bottom row: Evolution of the flow angle for four normalized bar passing time steps.

45°. The passage flow field receives alternating positive and negative fluctuations with an amplitude of about 5 % of the reference value. The streamline deformation of the wake passing through the passage is evident. The flow field angle outline the “negative jet” – effect. This effect, which is indicated by red color in the lower row of the figures, is a typical phenomenon in multistage turbomachinery as a consequence of the rotor wake / stator blade interaction. It was comprehensively studied by Hodson et al. 2012. The arrow heads indicate an alternating $\Delta\beta$ pointing from the pressure side of the lower blade towards the upper blade and vice versa. Specifically, the motion indicated by the larger arrow highlights the negative jet. This motion imposes an alternating fluid transport towards the suction side. Its orientations through the passage changes due to the high flow coefficient. At the position where the jet interacts with the suction side, it is periodically perturbing the wall-near boundary layer. Unfortunately, especially downstream of the passage’s throat, the suction side flow is prone to flow separation due to high loading and a decelerating boundary layer. Hence, the negative jet alternates the airfoil loading and periodically raises the risk of local flow separation. On the other hand, the periodically increased turbulence level triggers an earlier boundary layer transition (wake-induced transition), which increases the robustness against flow separation.

Finally, a comparison of the velocity fluctuations and the passage flow angles between the experiments and the numerical simulations is performed in Figure 9. The data for the time plot was exctracted at location P1 (x / C_x = 0.3) marked in the previous figures. A very good correlation for both, phase and amplitude, between experiments and CFD is highlighted.

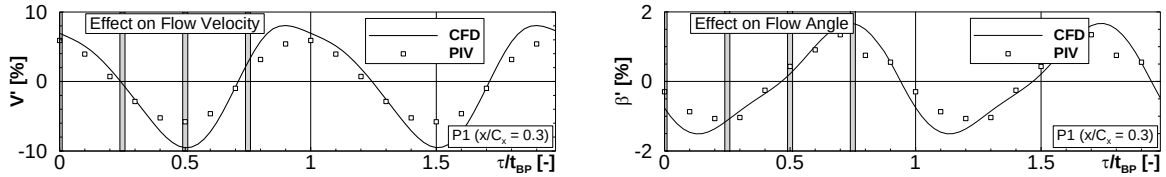

Figure 9: Effect of the bar wake on the secondary flow (z / H = 0.2) in the T106A turbine passage. Evolution of the bar wake effect at position *P1* over time for the velocity deficit and the flow angle - comparison between CFD and phase-locked PIV (grey positions in the time plot mark the displays in Figure 8).

GALA e.V., Karlsruhe, Germany, ISBN 978-3-9816764-9-5

Summary and Outlook

An experimental campaign was conducted on the T106A linear cascade with an additional endwall under challenging setup conditions. The primary goal of the experiments was to resolve the perturbated flow field in a blade-to-blade passage at mid-span and in the secondary flow regime close to an endwall. Phase-locked PIV measurements were applied to answer the question of how the passage flow field is distorted by the perturbations coming from periodically passing wakes. The wakes were generated by a wake generator equipped with cylindrical steel bars which pass by upstream of the cascade's leading edge with a frequency of 500 Hz.

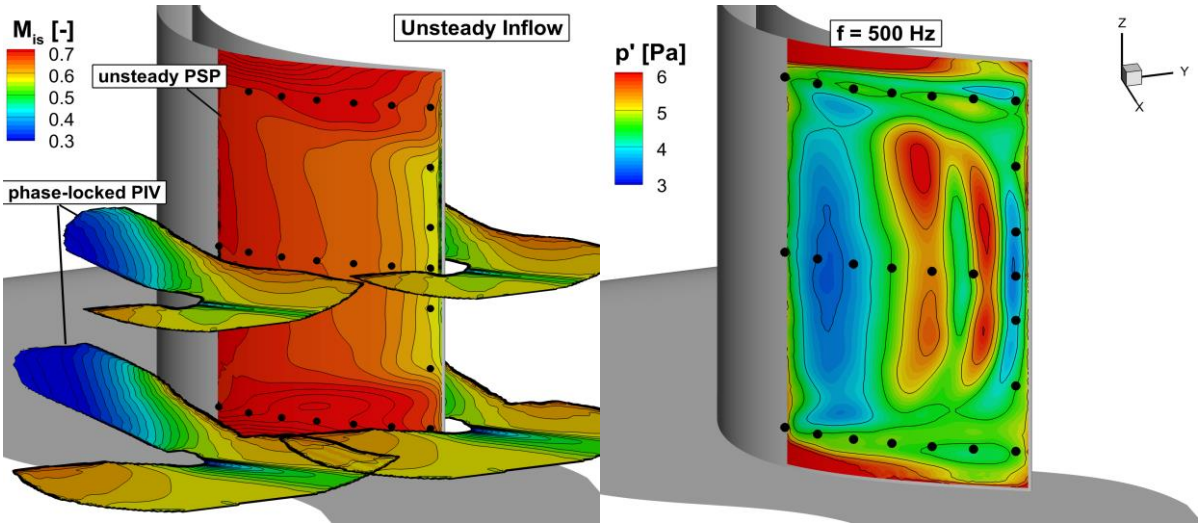

Figure 10: Illustration of the experimental dataset available for the T106A testcase under periodically disturbed inflow conditions. Left: Duplicated PIV passage flow fields presented in this paper and time-averaged isentropic surface Mach number on the blade's suction side from unsteady Pressure-Sensitive Paint measurement; right: high-resolution surface pressure amplitude measurement stimulated by the dominant wake generator frequency around 500 Hz. Black dots show markers for image mapping.

The comparison of the flow field topology inside the passage under steady versus unsteady conditions quantify the absolute wake-induced velocity difference between both. The higher deficit at unsteady conditions is linked to the total pressure losses produced by the bars of the wake generator. Nevertheless, the presence of unsteadiness leads to a reduction of the unavoidable underturning, especially in the secondary flow close to the endwall.

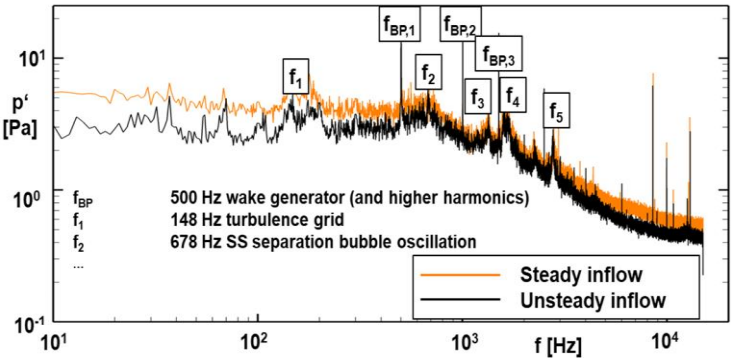

Figure 11: Pressure amplitude spectra from the blade's surface with (black) and without (orange) periodically incoming wakes measured with unsteady Pressure-Sensitive Paint technique using a high-speed camera sampled with 30 kHz.

The alternating amplification of the turbulence level inside the passage stemming from the bar wakes compensates negative effects, which may induce flow separation in particular from the blade's rear suction side surface. As part of the results, the nagative-jet effect was shown. Overall, the results are in good accordance with the numerical post-test predictions.

Apart from the results presented above, the comprehensive experimental dataset also comprises unsteady surface pressure data for comparison with the numerical data gathered in the project, compare Figures 10 & 11. The surface pressure data was measured with unsteady

GALA e.V., Karlsruhe, Germany, ISBN 978-3-9816764-9-5

Pressure-Sensitive Paint (i-PSP). The i-PSP measurements were performed using the intensity method, high-power uv-LED excitation and a high-speed camera sampled at 30 kHz. The pressure amplitudes from the right of Figure 10, which are typically very low under the ambient conditions inside the HGK test facility can be resolved precisely and correlate well with CFD. A view into the frequency spectra from Figure 11 allows the distinct identification of several dominant and secondary flow features up to several kilo-Hertz with or without the influence of the perodically incoming wakes. Unfortunately, the compre-hensive presentation and discussion of this dataset is far beyond the scope of this paper, but is in preparation for a follow-up publication.

Acknowledgements

The numerical design as well as the experimental investigations presented in this paper were performed in the framework of the joint project PAK 948 “Flow near the endwall of turbomachinery blading” funded by Deuchte Forschungsgemeinschaft under the funding code Ma 4922/8-1. The outstanding technical support provided by Mr. F. Grabendorfer and Mr. F. Burgstaller is also gratefully acknowledged.

References

Acton, P., Fottner L., 1996: “The generation of instationary flow conditions in the high-speed cascade wind tunnel”. in 13th Symposium on Measuring Techniques in Transonic and Supersonic Flow in Cascades and Turbomachines, September 5-6, Zürich, Switzerland.

Bear, P., Wolff, M., Gross, A., Marks, C. R., Sondergaard, R., 2018. “Experimental Investigation of Total Pressure Loss Development in a Highly Loaded Low-Pressure Turbine Cascade”. J. Turbomach. 140.

Bitter, M., Niehuis, R., 2019: “Effects of Periodic Inflow Turbulence on the Statistics in the Wake of a Linear LPT Cascade at Jet-Engine relevant Test Conditions”. 13th Int. Symp. Particle Image Velocimetry, 22.-24.7., Munich, Germany.

Blaim, F., Niehuis, R., 2012: “Unsteady Simulation of the LP Turbine Test Case T106D-EIZ using a Transport Equation based Transition Model”. Deutscher Luft- und Raumfahrtkongress, 10-12.9., Berlin, Germany.

Börner, M., Bitter, M., Niehuis, R., 2018: “On the Challenge of Five-Hole-Probe Measurements at High Subsonic Mach Numbers in the Wake of Transonic Turbine Cascades”. J. Glob. Power Propuls. Soc. 2018, pp. 453-464, DOI: 10.22261/JGPPS.JPRQQM.

Ciorciari, R., Kirik, I., Niehuis, R., 2014: “Effects of Unsteady Wakes on Secondary Flows in the Linear T106 Turbine Cascade”. J. Turbomach. 136(9), 091010, doi: 10.1115/1.4027374.

Ciorciari, R., Schubert, T., Niehuis, R., 2018: “Numerical Investigation of Secondary Flow and Loss Development in a Low Pressure Turbine Cascade with Divergent Endwalls”. J. Turbomach. Propuls. Power 2018, 3(1), 5.

Coull, J. D., 2017: “Endwall Loss in Turbine Cascades”. J. Turbomach. 139, doi: 10.1115/1.4035663.

Cui, J., Tucker, P. G., 2016: “Numerical Study of Purge and Secondary Flows in a Low Pressure Turbine”. ASME Paper No. GT2016-56789.

Denton, J., Pullan, G., 2012: “A Numerical Investigation into the Sources of Endwall Loss in Axial Flow Turbines”. ASME Paper No. GT2016-56350.

Engelmann, D., Sinkwitz, M., di Mare, F., Koppe, B., Mailach, R., Ventosa-Molina, J., Fröhlich, J., Schubert, T., Niehuis, R., 2021: “Near-Wall Flow in Turbomachinery Cascades – Results of a German Collaborative Project”. Int. J. Turbomach. Propuls. Power, 6, 9. doi: 10.3390/ijtpp6020009.

Hodson, H. P., Hynes, T. P., Greitzer, E. M., Tan, C. S., 2012: "A Physical Interpretation of Stagnation Pressure and Enthalpy Changes in Unsteady Flow." ASME. J. Turbomach. November 2012; 134(6).

Kampitsch, M., Stadtmüller, P., Fottner, L., 2000: “Investigations of Wake-Induced Transition on the LPT Cascades T106A-EIZ and T106D-EIZ”. ERCOFTAC Workshop, 19-23.3., La Clusaz, France.

GALA e.V., Karlsruhe, Germany, ISBN 978-3-9816764-9-5

Kirik, I., Niehuis, R., 2015: “Comparing the Effect of Unsteady Wakes on Parallel and Divergent End-walls in a LP Turbine Cascade (T106A-EIZ and T106D-EIZ)”. Proceedings of the 11th International Gas Turbine Congress, IGTC2015-137, 15.-20.11., Tokyo, Japan.

Langtry, R. B., Menter, F. R., 2005: “Transition Modeling for General CFD Applications in Aeronautics”. AIAA Paper 2005-522.

Niehuis, R., Bitter, M., 2021: “The High-Speed Cascade Wind Tunnel at the Bundeswehr University Munich after a Major Revision and Upgrade”. Int. J. Turbomach. Propuls. Power, 6, 41, doi: 10.3390/ijtpp6040041.

Schubert, T., Chemnitz, S., Niehuis, R., 2021: “The Effects of Inlet Boundary Layer Condition and Periodically Incoming Wakes on Secondary Flow in a Low Pressure Turbine Cascade”. ASME J. Turbomach., 143, 041001, doi: 10.1115/1.4050116.

Schubert, T., Niehuis, R., 2021: “Numerical Investigation of Loss Development in a Low-Pressure Turbine Cascade with Unsteady Inflow and Varying Inlet Endwall Boundary Layer”. In Proceedings of the ASME Turbo Expo, GT2021-59696, Virtual, Online, 7–11 June 2021, doi: 10.1115/GT2021-59606.

Volino, R., 2014: “Effects on Endwall Boundary Layer Thickness and Blade Tip Geometry on Flow through High Pressure Turbine Passages”. ASME Paper No. GT2014-27013.

Wilcox, D. C., 2004: “Turbulence Modeling for CFD (4th printing)”. DCW Industries, USA.

GALA e.V., Karlsruhe, Germany, ISBN 978-3-9816764-9-5